Available online at www.sciencedirect.com

SciVerse ScienceDirect

Ceramics International 38 (2012) 2325–2332

CERAMICS INTERNATIONAL

www.elsevier.com/locate/ceramint

# Structural, thermal, dielectric and ac conductivity properties of lithium fluoro-borate optical glasses

V. Naresh *, S. Buddhudu

*Department of Physics, Sri Venkateswara University, Tirupati 517502, India*

Received 13 October 2011; received in revised form 28 October 2011; accepted 31 October 2011
Available online 6 November 2011

**Abstract**

Transparent and stable glasses in the chemical composition of $Li_2O$–LiF–$B_2O_3$–MO (M = Zn and Cd) have been prepared by a conventional melt quenching method. For these glasses, absorption spectra, structural (XRD, FT-IR, and Raman spectra), thermal (TG–DTA and DSC), dielectric ($\varepsilon'$, $\varepsilon''$, tan $\delta$), ac conductivity ($\sigma_{ac}$), and electric modulus ($M'$ and $M''$) have been investigated. Amorphous nature of these glasses has been confirmed from their XRD profiles. The LFB glasses with the presence of ZnO or CdO an extended UV-transmission ability has been achieved. The measured FT-IR and Raman spectra have exhibited the vibrational bands of B–O from [$BO_3$] and [$BO_4$] units and Li–O. The dielectric properties (tan $\delta$, dielectric constant ($\varepsilon'$), dielectric loss ($\varepsilon''$)), electrical modulus and electrical conductivity ($\sigma_{ac}$) of these glasses have also been studied from 100 Hz to 1 MHz at the room temperature. Based on the trends noticed in the ac conductivities, the present glasses could be found useful as battery cathode materials.



*Keywords:* Glasses; Dielectric; Conductivity analysis

## 1. Introduction

Significance and importance of glassy materials over the crystalline materials have earlier been reported in the literature [1,2]. It has been observed that certain borate glasses are of greater interest and relevance because of their suitability in the progress of waveguides, electro-optic switches and modulators, magneto-optic materials, solid state laser materials and optical parametric devices [3–6]. In the literature, optical materials containing $Li^+$ ions have widely been studied [7–10] for their use in various applications. In order to further promote $Li^+$ ions containing borate glasses as UV-transmitting, transparent and more stable systems, presence of LiF in such glasses, has also been recognised [11–14]. In the present work, we propose to add ZnO or CdO in the chemical composition of $Li_2O$–LiF–$B_2O_3$ based glasses to achieve further betterment in their UV transmission abilities and also enhancement of their conductivity properties.

## 2. Experimental studies

Preparation of the glasses has been shown in the form of a flow chart in Fig. 1. Lithium fluoro-borate (LFB) glasses containing metal oxides (ZnO or CdO) have been prepared by melt quenching method. The starting chemicals used were in analytical grade such as $H_3BO_3$, $Li_2CO_3$, LiF, $ZnCO_3$, and $CdCO_3$. All the chemicals were weighed in 10 g batch each separately, thoroughly mixed using an agate mortar and a pestle and then each of those was collected into porcelain crucible and pre-heated in an electric furnace at 450–500 °C for about half an hour. Such pre-heated chemicals batches were transferred into separate porcelain crucibles for melting them for an hour at 950 °C. These melts were quench in between two smooth surface brass plates to obtain glasses in circular designs with 2–3 cm in diameter and a thickness of 0.3 cm as shown in Fig. 2. For an easy reference, these glasses have been labelled as LFB, LFBZn, LFBCd as presented in Table 1.

Absorption spectra of glasses (Fig. 3) were measured on a Varian-Cary-Win Spectrometer (JASCO V-570). Simultaneous measurement of TGA and DTA was carried out (Fig. 4(a)) on NetZsch STA 409 at a heating rate of 10 °C/min with $N_2$ as the purging gas and the DSC profile was also obtained (Fig. 4(b)) to

* Corresponding author.
*E-mail addresses:* varna.narseh@gmail.com (V. Naresh), svuniv@hotmail.com (S. Buddhudu).

0272-8842/$36.00 
doi:10.1016/j.ceramint.2011.10.084

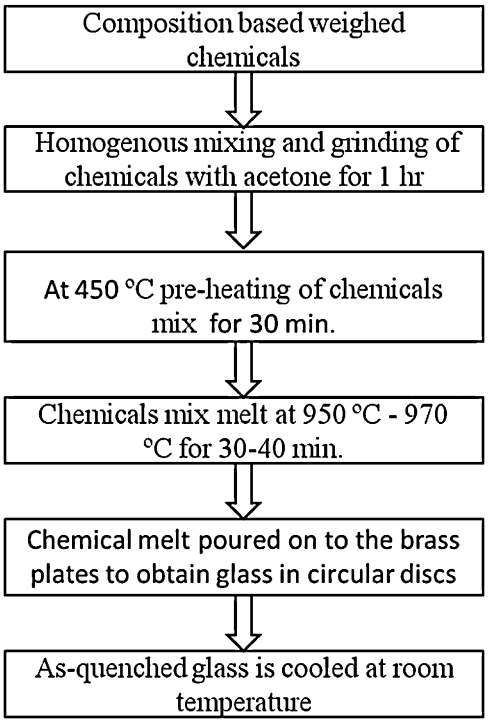


Fig. 1. Sample preperation describing flow chart.

correlate both DTA and DSC results for a better understanding of the trends. XRD profiles were recorded on a Seifert X-ray Diffractometer (model 3003TT) with Cu $K_\alpha$ radiation ($\lambda = 1.5406$ Å) at 40 kV and 20 mA with a Si detector and $2\theta = 10^\circ$ and $60^\circ$ at the rate of two degrees per minute. FT-IR spectrum of the sample was recorded on a Nicolet-5700 FT-IR spectrometer using KBr pellet technique in the range of 4000–400 $cm^{-1}$. Raman spectrum was measured using Jobin Yvon Horiba (LABRAM HR – 800) Micro Raman spectrometer attached with an $Ar^+$ laser (488 nm) as the excitation source having an output power of 15 mW with a laser beam spot size as 100 μm by employing an appropriate lens system. Dielectric profiles of the glasses at room temperature were measured in the frequency range of 100 Hz to 1 MHz on a Phase Sensitive Multimeter (PSM 1700) in LCR mode.

## 3. Results and discussion

From the optical absorption spectra (Fig. 3) it is observed that these glasses have transmission ability, the absorption edge has shifted this is attributed to the displacement of oxygen from its normal position resulting in the formation of Non-Bridging

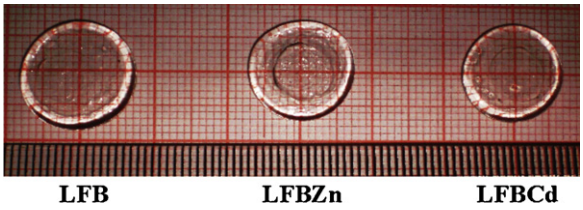


Fig. 2. $Li_2O$–LiF–$B_2O_3$–MO glasses, where M = Zn and Cd.

Table 1
Chemical compositions of glass systems.

| Glass abbreviations | Chemical compositions |
|---|---|
| LFB | $30Li_2O$–20LiF–$50B_2O_3$ |
| LFBZn | $30Li_2O$–20LiF–4ZnO–$46B_2O_3$ |
| LFBCd | $30Li_2O$–20LiF–4CdO–$46B_2O_3$ |

Oxygens (NBOs), which could shift the absorption edge to lower energies.

In Fig. 4(a), the TG profile has shown that the weight loss of the sample has been in a multistep process in the temperature range of 39–700 °C. The initial weight loss of sample takes place between 39 °C and 130 °C due to the decomposition of the organic compounds that were used during the grinding of the chemicals mix [15], the observed weight loss has been at 4.6%. The second weight loss has been noticed in the temperature range of 130–176 °C, due to the transformation of boric acid ($H_3BO_3$) at 130 °C into meta-boric acid ($HBO_2$), which crystallizes in three different forms: α-$HBO_2$ (orthorhombic), β-$HBO_2$ (monoclinic), and γ-$HBO_2$ (cubic). Among them, the cubic (γ-$HBO_2$) phase is reported to be stable; with a weight loss of 8%. Upon further heating, the third weight loss has occurred in the temperature range of 176–460 °C because of the conversion of $HBO_2$ as tetraboric acid or pyroboric acid, which in turn becomes as an anhydrous oxide $B_2O_3$ in crystalline form that melts at 460 °C, the weight loss there has been at 7.6%. The final weight loss in the range of 460–590 °C due to the decomposition of $Li_2CO_3$ into $Li_2O$ and $CO_2$ with such elimination, the weight loss is about 15.4%. There has been no significant weight loss beyond 600 °C as is seen from the TG profile of the LFB glass precursor chemicals. From Fig. 4(a) and (b), two sharp exothermic peaks have been observed which reveals the chemical reaction at 159 °C and 569 °C. The peak at 159 °C is attributed to the short range order and partial melting of small percentage of impurity phase [16] and phase changes, the other peak at 569 °C is due to the heat loss during the crystallization, which is the peak at the crystallization temperature ($T_c$), and the onset of crystalline

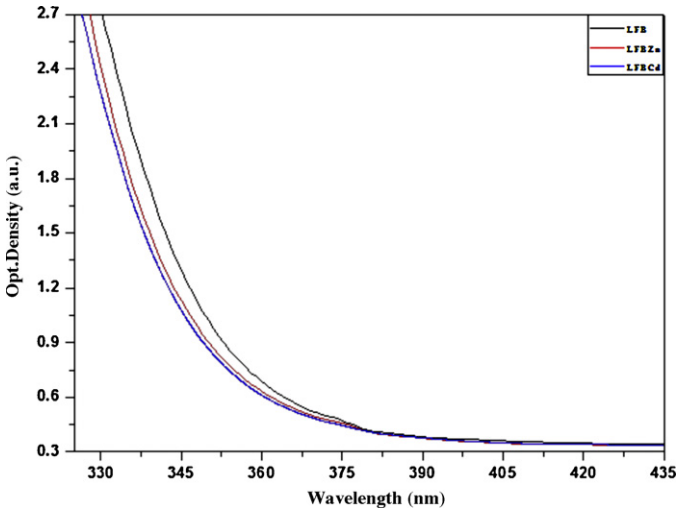


Fig. 3. Absorption spectra of LFB and LFBMO glasses, where M = Zn and Cd.

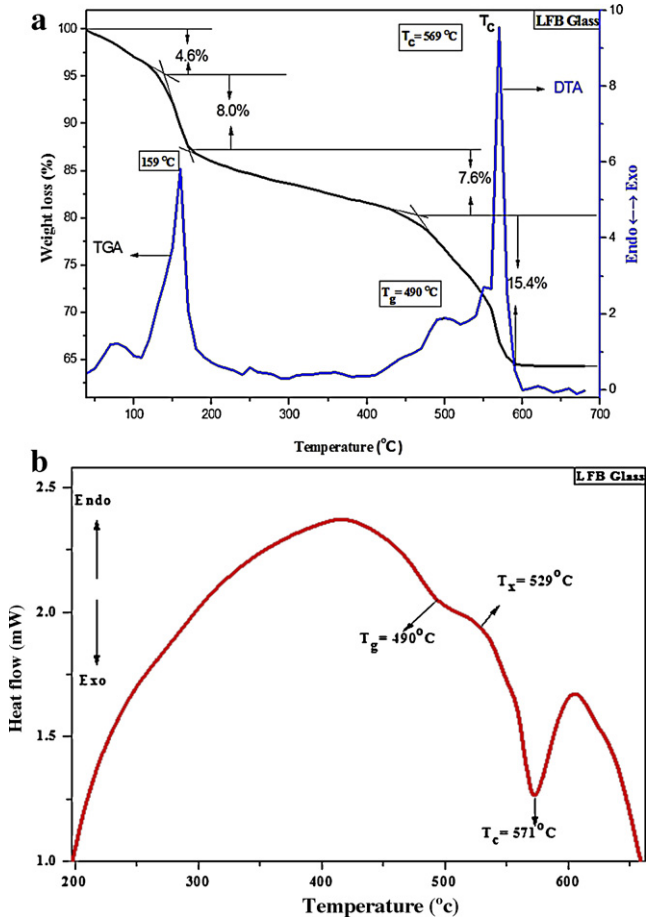


Fig. 4. (a) TG–DTA profiles of the LFB ($Li_2O$–LiF–$B_2O_3$) precursor chemicals. (b) DSC profile of the LFB ($Li_2O$–LiF–$B_2O_3$) precursor chemicals.

temperature ($T_x$) exists at 529 °C, the glass transition temperature ($T_g$) is 490 °C. The peak crystallization temperature ($T_c$) and the glass transition temperature ($T_g$) for the very same sample precursor in its DTA profile has been correlated with its DSC profile.

In Fig. 5, XRD profiles reveals a broad hollow band (diffused peak) at 2$\theta$ (10–20°) could been noticed in all glass samples,

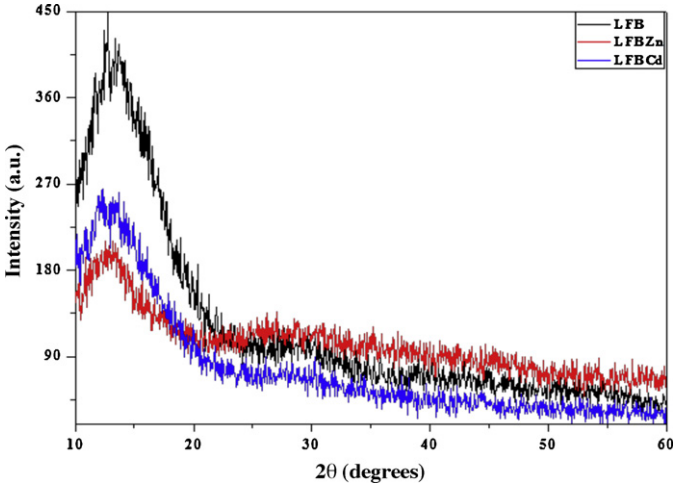


Fig. 5. XRD profiles of LFB and LFBMO glasses, where M = Zn and Cd.

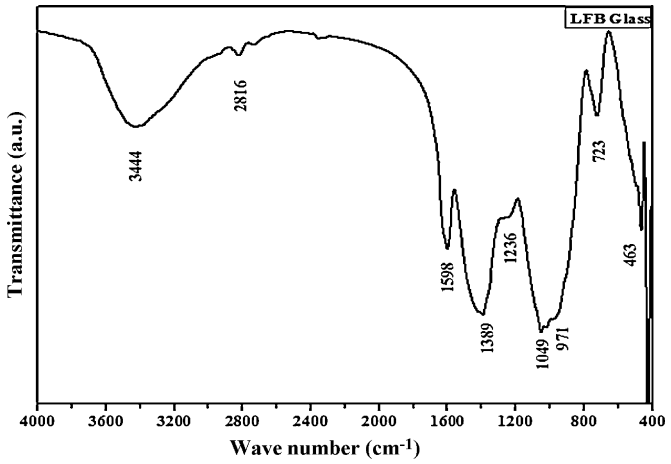


Fig. 6. FT-IR spectrum of LFB ($Li_2O$–LiF–$B_2O_3$) glass.

which clearly indicates their amorphous nature. Fig. 6 presents the FT-IR spectrum of LFB ($Li_2O$–LiF–$B_2O_3$) glass, describing the structure of vitreous borate consisting of random network of $BO_3$ triangles with certain fraction of boroxol (six membered) rings but with the inclusion of the network modifier such as alkaline/alkaline earth metals, formation of $BO_4$ network modifier takes place in the borate glass network. The FT-IR has shown characteristic peaks at 463 $cm^{-1}$, 723 $cm^{-1}$, 971 $cm^{-1}$, 1049 $cm^{-1}$, 1236 $cm^{-1}$, 1395 $cm^{-1}$, 1598 $cm^{-1}$, 2816 $cm^{-1}$ and 3444 $cm^{-1}$. The broad bands are due to the combination of factors such as high degeneracy of vibrational state, thermal broadening of lattice dispersion band and also mechanical scattering in the glass. In the infrared spectral region, the vibrational modes of borate show three regions [17], the first region at 1200–1600 $cm^{-1}$ band is due to an asymmetric stretching of relaxation of the B–O bond of trigonal $BO_3$ units, the second region at 800–1200 $cm^{-1}$ due to the B–O bond stretching of tetrahedral $BO_4$ units, and third region bands at 600–800 $cm^{-1}$ is originating from the bending vibrations of B–O–B linkages in borate network [18]. In the present glass, the absence of peak at 806 $cm^{-1}$ indicates the absence of boroxol ring. The substitution of boroxol rings by triborate and tetraborate groups has been observed. The band at 463 $cm^{-1}$ is assigned to the characteristic vibration of lithium cation [19]. The band at 723 $cm^{-1}$ is due to the bending vibrations of B–O–B linkage in the borate network [20]. A small band at 971 $cm^{-1}$ and another band at 1049 $cm^{-1}$, is due to the stretching vibrations of B–O in $BO_4$ units from tri-, tetra-, and penta borate groups [21]. The band at 1236 $cm^{-1}$ is attributed to the asymmetric stretching vibrations of $O^-$–B bonds from orthoborate groups. The band at 1236 $cm^{-1}$ indicates the presence of $BO_3$ unit with non-bridging oxygen existing in boron oxygen network [22]. The band at 1395 $cm^{-1}$ is due to the stretching of B–O bonds of various borate arrangements containing planar six membered borate groups, exhibiting a compositional dependence that originates from different species. The peak at 1598 $cm^{-1}$ is raised from B–O stretching vibrations of $[BO_3]^{3-}$ units [23]. The band at 2816 $cm^{-1}$ can be attributed to Hydrogen bonds and a broad band at 3444 $cm^{-1}$ is due to the hydroxyl group (due to stretching of $OH^-$) [24]. The

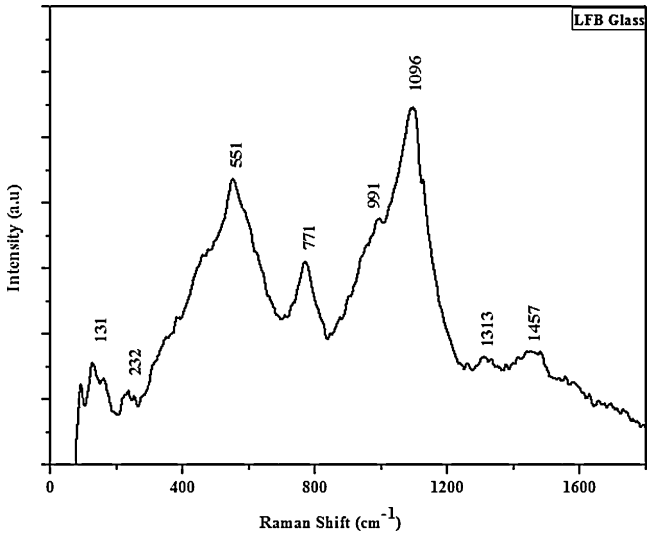


Fig. 7. Raman spectrum of LFB ($Li_2O$–LiF–$B_2O_3$) glass.

contribution due to borate network dynamics is mostly in the mid-infrared region of the profile, where as for lithium cation motion dominates in the low frequency region. Thus, LFB glass without ZnO and CdO has demonstrated the presence of the principle bands at the three regions.

Raman spectrum of LFB glass is shown in Fig. 7 exhibiting bands at 131 $cm^{-1}$, 232 $cm^{-1}$, 551 $cm^{-1}$, 771 $cm^{-1}$, 991 $cm^{-1}$, 1096 $cm^{-1}$, 1313 $cm^{-1}$, and 1457 $cm^{-1}$. It is reported that pure $B_2O_3$ reveals a strong band at 806 $cm^{-1}$ and which is assigned to the boroxol ring oxygen breathing vibrations involving a very little boron motion [25,26]. In the LFB glass, with the availability of $Li_2O$ (>30%), the $B_2O_3$ transforms into a complex network which involves a boroxol ring coupled with a fourfold-coordinated boron ($BO_4$) because of the non-bridging oxygens. The peak at 771 $cm^{-1}$ is assigned due to breathing vibrations of a six member rings with $BO_3$ triangles replaced by $BO_4$ tetrahedral units [27–29]. The band at 553 $cm^{-1}$ is attributed to a bending mode (B–O–B) of $BO_3^{3-}$ units [30]. The peak at 991 $cm^{-1}$ is due to a di-borate group [31] and the peak at 1096 $cm^{-1}$ is due to the vibrations of di-borate groups formed from six membered rings that contain two $BO_4$ tetrahedral units in the structure [32–34]. The peaks in the higher frequency region are due to $BO_2O^-$ triangles linked to $BO_4$ units and $BO_2O^-$ triangles linked to other triangular units [35,36]. In the lower frequency range, a peak is observed in the lithium borate glass at 131 $cm^{-1}$ that could be attributed to liberational mode of $BO_3$ and $BO_4$ units [37]. Two broader peaks at 1313 $cm^{-1}$ and 1457 $cm^{-1}$ are because of the overlap of different modes such as: (i) B–$O^-$ in $BO_2O^-$, (ii) $BO_2O^-$ triangles linked to $BO_4$ units and (iii) stretching in $BO_3$ triangles which are asymmetrically connected [38,39].

A variety of anionic borate groups like di-, tri-, tetra-, penta-, pyro-, ortho-, and meta-borates have been identified in the glass studied here. Tables 2 and 3 show the peak positions with appropriate assignments pertaining to the measured FT-IR and Raman spectral profiles of the LFB glass.

Dielectric properties of ionic conducting glasses are due to the contribution of electronic, ionic, dipole orientations and space charge polarizations. The charge carriers in a glass cannot move freely through but those could be displaced and thus become polarized depending upon applied alternating field. The complex permittivity of the glass is obtained from the impedance data:

$$\varepsilon^* = \frac{1}{(j\omega C_o Z^*)} = \varepsilon' - j\varepsilon'' \quad (1)$$

where $Z^*$ is the complex impedance, $C_o$ is the capacitance of free medium. The real part of permittivity (dielectric constant) $\varepsilon'$ represents the polarizability, while the imaginary part (dielectric loss) $\varepsilon''$ represents the energy loss due to polarization and ionic conduction. The dielectric constant ($\varepsilon'$) is calculated from:

$$\varepsilon' = \frac{Cd}{\varepsilon_o A} \quad (2)$$

where $C$ is the capacitance of the sample, $\varepsilon_o$ is the permittivity of the free space ($8.85 \times 10^{-12}$ F/m) and $A$ is the cross-sectional area of electrode and dielectric loss tangent is evaluated from

$$\tan\delta = \frac{\varepsilon''}{\varepsilon'} \quad (3)$$

where $\tan\delta$ is the loss tangent. The ac conductivity of the sample ($\sigma_{ac}$) is determined from:

$$\sigma_{ac} = \omega\varepsilon_o\varepsilon'' \quad (4)$$

where $\omega$ is the angular frequency.

Table 2
Assignment of measured FT-IR band positions of LFB ($Li_2O$–LiF–$B_2O_3$) glass.

| Band positions ($cm^{-1}$) | | Assignments | Refs. |
|---|---|---|---|
| Measured | Literature | | |
| 463 | 450 | Bending vibrations of Li–O and $BO_4$ units | [20] |
| 723 | 720 | $BO_3$–O–$BO_3$ bond bending vibrations | [22] |
| 971 | 900–1000 | Asymmetric vibration of B–O bonds in $BO_4$ | [24] |
| 1049 | 1040 | B–O stretch in $BO_4$ units from tri-, tetra, and penta borate groups | |
| | 1060 | | [20,21,26] |
| 1236 | 1235 | B–O stretching vibrations of $(BO_3)^{3-}$ units in ortho-borate chains | [21,22] |
| 1395 | 1402 | B–$O^-$ asymmetry stretching modes of $BO_3$ triangular and $BO_2O^-$ units | [23] |
| 1598 | 1559 | B–$O^-$ stretching vibration of triangle $(BO_3)^{3-}$ from various types of borate groups | [23,25] |
| 2816 | 2700–2850 | Attributed to hydrogen bonds (O–H stretching vibration) | [24] |
| 3444 | 3429–3466 | Attributed to hydroxyl bonds | [24] |

Table 3
Assignment of measured Raman band positions of LFB ($Li_2O$–LiF–$B_2O_3$) glass.

| Band positions ($cm^{-1}$) | | Assignments | Refs. |
|---|---|---|---|
| Measured | Literature | | |
| 131 | 135 | Liberational modes of $BO_3$ and $BO_4$ units | [37] |
| 553 | 548 | In plane – bending mode of $BO_3^{3-}$ units | [27] |
| 771 | 760–780 | Ring breathing vibration of six membered ring containing both $BO_3$ triangles and $BO_4$ tetrahedral | [27] |
| 991 | 950 | Due to penta borate and tetraborate group | [26,27] |
| | 980 | | |
| 1094 | 1110 | Due to diborate group | [26,32,33] |
| | 1050 | | |
| 1313 | 1380 | Due to $BO_2O^-$ triangles linked to BO units | [22,38] |
| 1457 | 1490 | Band is attributed to triangles linked to other borateborate triangular units | [22,38] |

In Fig. 8(a), it is observed that dielectric constant ($\varepsilon'(\omega)$) values are decreased with an increase in frequency and reaches to a minimum value without any further decrease from 100 kHz to 1 MHz because of the accumulation of space charge near the electrode–electrolyte interface due to polarization. Therefore, at higher frequency region dielectric constant ($\varepsilon'(\omega)$) follows a non-Debye behaviour $\omega^{-(1-s)}$ [40–42]. From Fig. 8(b), dielectric loss tangent has high dispersion at low frequency, which decreases gradually as frequency increases due to less contribution of ions in the direction of applied electric field.

From the profiles of dielectric constant ($\varepsilon'$) and loss tangent ($\tan\delta$) as a function of $\log(\omega)$, it is noticed that there exists a small shoulder appears at 10 kHz for the glasses studied, which could be due to the bulk polarization, where immobile and mobile ions cannot oscillate as the applied field, and therefore dispersion takes place as a result of rapid polarization process [43–45].

Fig. 9 shows the frequency dependent ac conductivity plots of $\log\sigma_{ac}$ versus $\log(\omega)$ at the room temperature for the glasses studied here based on Jonscher universal power law [46]:

$$\sigma(\omega) = \sigma_{dc} + A\omega^s, \quad 0 < s < 1 \tag{5}$$

where $\sigma_{dc}$ is the dc conductivity of the samples, $A = (\sigma_{dc}/\omega_p^s)$ is temperature dependent constant, $\omega = 2\pi f$ is the angular frequency of the applied field and $s$ is the power law exponent in the range $0 < s < 1$, represents the degree of interaction between the mobile ions. The frequency dependence of conductivity is sum of the dc conductivity due to movements of free charges and polarization conductivity (ac conductivity) due to movements of bound charges. It is observed from the $\log\sigma_{ac}$

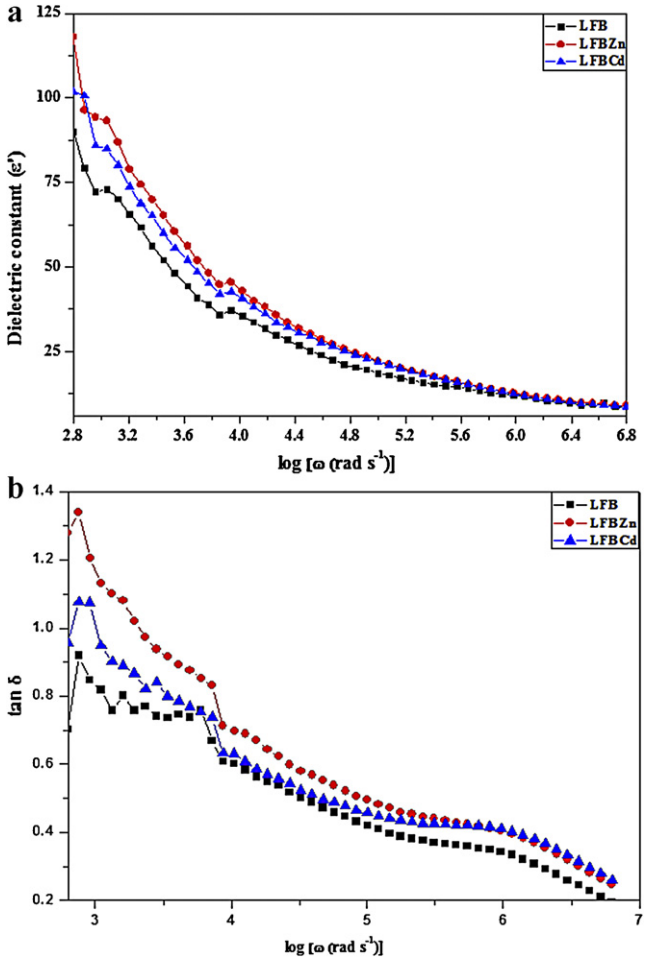


Fig. 8. (a) Dielectric constant ($\varepsilon'$) as a function of $\log(\omega)$ at room temperature for LFB and LFBMO (M = Zn and Cd) glasses. (b) Variation of dielectric loss factor ($\varepsilon''$) with $\log(\omega)$ at room temperature for LFB and LFBMO glasses, where M = Zn and Cd.

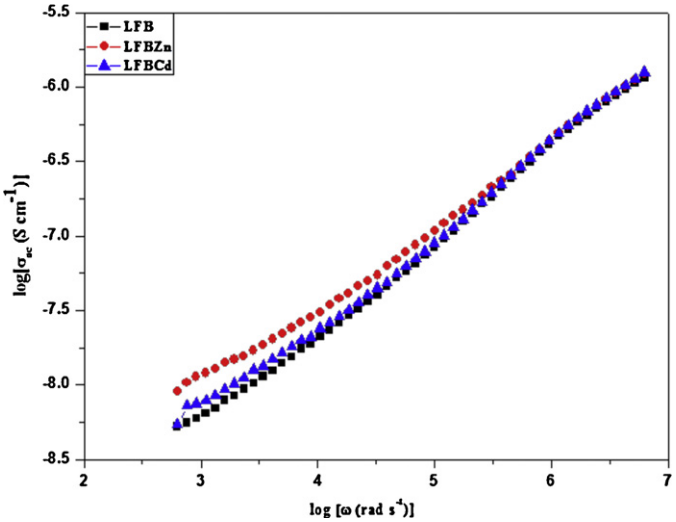


Fig. 9. Conductivities ($\log\sigma_{ac}$) as function of $\log(\omega)$ at room temperature for LFB and LFBMO (M = Zn and Cd) glasses.

Table 4
The conductivity values for LFB and LFBMO glass systems, where M = Zn, Cd.

| Glass abbreviation | Ac conductivity (S/cm) | *s*-Value |
|---|---|---|
| LFB | $1.19 \times 10^{-6}$ | 0.61 |
| LFBZn | $1.22 \times 10^{-6}$ | 0.63 |
| LFBCd | $1.24 \times 10^{-6}$ | 0.68 |

versus log $\omega$ plots, the dc plateau disappears due to the electrode polarization effects found to cover-up the dc conductivity plateau region in the lower frequency range. The conductivity curves were tending to merge into a single curve becoming strongly frequency dependent; these curves show almost a linear behaviour that follows a power law relation:

$$\sigma(\omega) = A\omega^s, \quad s < 1 \tag{6}$$

The values of the exponent $s$ is obtained from the slopes of log $\sigma_{ac}$ ($\omega$) versus log $\omega$ for the curves on the theoretical lines as fitted by Eq. (5) using the equation $S = (d(\ln \sigma_{ac}(\omega))/d(\ln(\omega)))$ at room temperature for all compositions [47]. The parameter $s$ is associated with the modification of network structure and its smaller value signifies the higher degree of modification, in the present case the composition with Zn (0.61) and Cd (0.68), are found to have less $s$ (<1) value, whose degree of modification could be higher [48]. The ac conductivity for glass systems is given in Table 4.

Fig. 9 shows the profiles of the ac conductivity of the glasses reported here revealing an increasing trend in the conductivity with the change of frequency, which is due to an increased density of mobile ions for conduction. The ac conductivity is found to be independent at lower frequencies, however, with an increase in frequency, the ac conductivity sets in and approaches close to a frequency power law with exponent < 1 and it characterizes the non-Debye feature [49].

Following the reports of Macedo et al. [50], complex electrical modulus ($M^*$) could be defined as the electrical analogue of the dynamical mechanical modulus of complex dielectric constant ($\varepsilon^*$) represented as:

$$M^* = \frac{1}{\varepsilon^*} \tag{7}$$

$$M^* = M' + jM'' = \frac{\varepsilon'}{(\varepsilon')^2 + (\varepsilon'')^2} + j\frac{\varepsilon''}{(\varepsilon')^2 + (\varepsilon'')^2} \tag{8}$$

where $M'$, $M''$ and $\varepsilon'$, $\varepsilon''$ are the real and imaginary parts of modulus and dielectric constants respectively. The profiles of $M'$ and $M''$ at room temperature are shown in Fig. 10(a) and (b). The $M'$ profiles in Fig. 10(a) reveal that the curves almost tends to zero in the low frequency range at the room temperature. It is due to the suppression of electrode polarization, while at higher frequencies it reaches $M'_\infty (= 1/\varepsilon_\infty)$ because of the distribution of relaxation processes over a range of frequencies. In Fig. 10(b), it is observed that the shape of the each $M''$ curve is broader than ideal Debye curves and asymmetric in nature with variation in peak height (FWHM) exhibiting a relaxation peak at characteristic relaxation frequency ($\omega_m$). In the lower

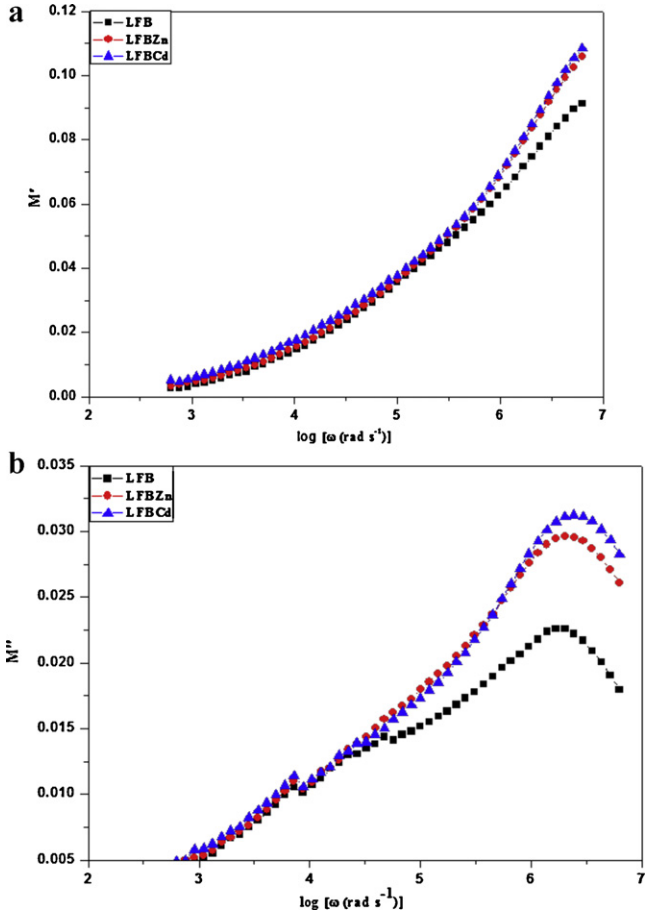


Fig. 10. (a) Dependence of real electrical modulus ($M'$) results as function of log($\omega$) at room temperature for LFB and LFBMO (M = Zn and Cd) glasses. (b) Dependence of imaginary electrical modulus ($M''$) with log($\omega$) at constant temperature for LFB and LFBMO (M = Zn and Cd) glasses.

frequency region, the ions drift to long distances, and at higher frequency region, the ions drift to short distances or spatially localized. In the frequency region where the peak occurs is due to the transition from the long-range to short-range ion mobility.

The relaxation behaviour is observed to be non-Debye type, which could be due to the amorphous nature of glasses and distribution of the (Zn and Cd) oxide ionic sites within the glasses to which the ionic jump occurs [51]. As the interaction among the charge carriers become prominent, the effect of inter-ionic interaction and correlation among the ions come into play and in turn govern the relaxation behaviour due to the availability of non-bridging oxygen sites in the glass [52].

The traces of electric modulus formalism reveal that the relaxation peaks which are suppressed in the case of dielectric loss tangent due to accumulation of charges are prominent in this plots and also the ions diffuse through longer distance in the $M''$ spectra.

## 4. Conclusion

In brief, it is concluded that, the LFB ($Li_2O$–LiF–$B_2O_3$) and LFBMO (M = ZnO, and CdO) glasses have successfully been prepared. The optical absorption, XRD, TG–DTA, DSC, FT-IR

and Raman spectral results have been investigated for the LFB glass to analyze its thermal and structural properties. From optical absorption spectra of LFB and LFBMO glasses, it is observed that with the presence of ZnO or CdO in LFB glass matrix, UV transmission ability has been enhanced and such glasses possess good strengths. The dielectric properties are measured for the LFB and LFBMO glasses, it is observed that because of dielectric properties are decreasing with an increase in the frequency because, the dipoles are no longer able to orient rapidly so that their oscillations begin to lag behind those of electric field in the glasses studied. A small increase in ac conductivity is observed with the addition of (Zn/Cd) in the LFB glass. The values of '*s*' are also calculated in evaluating the degree of interaction of ions in the glasses.

## References


[1] B.V.R. Chowdari, R. Zhou, Study of the fluorinated lithium borate glasses, Solid State Ionics 78 (1995) 133–142.

[2] S. Lee, M. Lee, K.J. Lim, Femtosecond laser induced PL change in Sm-doped sodium borate glass and 3D optical memory, J. Lumin. 122–123 (2007) 990–992.

[3] A. Paul, R.W. Douglas, Cerous-ceric equilibrium in binary alkali borate and alkali silicate glasses, Phys. Chem. Glasses 6 (1965) 212–215.

[4] J.L. Piguet, J.E. Shelby, preparation and properties of silver borate glasses, J. Am. Ceram. Soc. 68 (1985) 450.

[5] I.W. Donald, B.L. Metcalfe, D.J. Bradley, M.J.C. Hill, J.L. McGrath, A.D. Bye, The preparation and properties of some lithium borate based glasses, J. Mater. Sci. 29 (1994) 6379.

[6] Y.L. Yue, X.J. Yu, H.T. Wu, X.J. Chen, Dielectric properties of quaternary calcium aluminoborosilicate system glasses, Mater. Res. Innovations 13 (2009) 129.

[7] M.A. Baki, F. Abde-Wahab, F. El-Diasty, Factor affecting optical dispersion in borate glass systems, J. Phys. Chem. Solids 68 (2007) 1457–1470.

[8] G. Venkateswara Rao, N. Veeraiah, P.Y. Reddy, Luminescence quenching by manganese ions in MO–$CaF_2$–$B_2O_3$ glasses, Opt. Mater. 22 (2003) 295.

[9] S. Khasa, V.P. Seth, A. Agarval, S.K. Gupta, Effect of nickel ions on electron paramagnetic resonance, DC conductivity and thermal behavior in vanadyl doped $NiO{\cdot}Li_2O{\cdot}B_2O_3$ glasses, Mater. Chem. Phys. 72 (2001) 366–373.

[10] T.D. Tho, R.P. Rao, S. Adams, Glass formation, structure and ion transport in $0.45Li_2O$–$(0.55 - x)P_2O_5$–$xB_2O_3$ glasses, Phys. Chem. Glasses: Eur. J. Glass Sci. Technol. B 52 (3) (2011) 91–100.

[11] B. Sridhar, B. Indira, A.K. Bhatnagar, Electron Paramagnetic Resonance spectra of transition metal and rare-earth ions in lithium fluoroborate glasses, Indian J. Pure Appl. Phys. 33 (1995) 353–356.

[12] P. Babu, C.K. Jaysankar, Optical spectroscopy of $Eu^{3+}$ ions in lithium borate and lithium fuoroborate glasses, Physica B 279 (2000) 262–281.

[13] L.R.D. Kassab, L.C. Courrol, A.S. Morais, i.S.H. Tatum, N.U. Wetter, L. Gomes, Spectroscopic properties of lead fluoroborate glasses codoped with $Er^{3+}$ and $Yb^{3+}$, J. Opt. Soc. Am. B 19 (2002) 2921.

[14] J. Senegas, J.M. Reau, H. Aomi, P. Hagenmuller, M. Poulain, Ionic conductivity and NMR investigation of quaternary glasses in the $ZrF_4{\cdot}BaF_2{\cdot}ThF_4{\cdot}LiF$ system, J. Non-Cryst. Solids 85 (1986) 315–334.

[15] A. Ngamjarurojana, O. Khamman, Yimnirun, S. Ananta, Effect of calcinations on phase formation and particle size of Zinc niobate powders synthesized by solid-state reaction, Mater. Lett. 60 (2006) 2867–2872.

[16] K. Singh, D. Bahadur, Stability and phase transition in $Al_{65}{\cdot}Cu_{20}{\cdot}Co_{15-x}{\cdot}Fe_x$, Indian J. Pure Appl. Phys. 46 (2008) 497–501.

[17] Y.B. Saddeek, H.A. Afifi, N.S. Abd El-Aal, Interpretation of mechanical properties and structure of $TeO_2$–$Li_2O$–$B_2O_3$ glasses, Physica B 398 (2007) 1.

[18] B.V. Rao, U. Rambabau, S. Buddhudu, B.V. Rao, U. Rambabau, S. Buddhudu, Photoluminescence spectral analysis of $Eu^{3+}$: phosphors, Physica B 382 (2006) 86–91.

[19] T. Raghavendra Rao, C. Rama Krishna, C. Venkata Reddy, U.S. Udayachandran Thampy, Y.P. Reddy, P.S. Rao, R.V.S.S.N. Ravikumar, Mixed alkali effect and optical properties of $Ni^{2+}$ doped $20ZnO + x$-$Li_2O + (30 - x)Na_2O + 50B_2O_3$ glasses, Spectrochim. Acta A 79 (2011) 1116–1122.

[20] R. Lal, N.D. Sharma, Infrared spectroscopic study of zinc doped iron borate glasses, Indian J. Pure Appl. Phys. 43 (2005) 828–832.

[21] E.I. Kamitsos, G.D. Chryssikos, Borate glass structure by Raman and infrared spectroscopies, J. Mol. Spectrosc. 247 (1991) 1–16.

[22] G. Padmaja, P. Kistaiah, Infrared and Raman spectroscopic studies on alkali borate glasses: evidence of mixed alkali effect, J. Phys. Chem. A 113 (2009) 2397–2404.

[23] E.I. Kamitsos, M.A. Karakassideaand, G.D. Chyrssikos, A vibrational study of lithium borate glasses with high $Li_2O$ content, J. Phys. Chem. 91 (1987) 1073–1079.

[24] S. Suresh, M. Prasad, G. Upender, V. Kamalaker, V. Chandra Mouli, ESR, IR, Raman and optical absorption studies of $60B_2O_3 + 10TeO_2 + 5$-$TiO_2 + 24R_2O$: 1CuO (where R = Li, Na, K) quaternary glasses, Indian J. Pure Appl. Phys. 47 (2009) 163–169.

[25] J. Krogh-Moe, Interpretation of the infra-red spectra of boron oxide and alkali borate glasses, Phys. Chem. Glasses 6 (1965) 46.

[26] F.L. Galneer, Planar rings in glasses, Solid State Commun. 44 (1982) 1037.

[27] B.P. Dwivedi, B.N. Khanna, Cation dependence of Raman scattering in alkali borate glasses, J. Phys. Chem. Solids 56 (1) (1995) 39–49.

[28] T.W. Brill, Philips Res. Rep. Suppl. 1 (1975) 1.

[29] W.L. Koijnendijk, Structure of glasses in the system CaO–$Na_2O$–$B_2O_3$ and MgO–$Na_2O$–$B_2O_3$ studied by raman scattering, Phys. Chem. Glasses 17 (1976) 205.

[30] Y.D. Yiannopoulos, G.D. Chryssikos, E.I. Kamitsos, Structure and properties of alkaline earth borate glasses, Phys. Chem. Glasses 42 (2001) 164.

[31] W.L. Konijnendijk, Structure of borosilicate glasses, Philips Res. Rep. Suppl. 1 (1975) 243.

[32] D. Maniu, I. Ardelean, T. Iliescu, S. Cinta, V. Nagel, W. Kiefer, Raman spectroscopic investigations on oxide glass system $(1 - x)[3B_2O_3K_2O]{\cdot}xTiO_2$, J. Mol. Struct. 657 (1999) 480–481.

[33] T.W. Bril, Raman spectroscopy of crystalline and vitreous borates, Philips Res. Rep. Suppl. 2 (1976) 117.

[34] B.N. Meera, N. Chandrabhas, A.K. Sood, Raman study of lead borate glass, J. Non-Cryst. Solids 126 (1990) 224.

[35] A. Ryichi, O. Norikazu, U. Norimasa, Raman spectra of $K_2O$–$B_2O_3$ glasses and melts, J. Non-Cryst. Solids 293–295 (2001) 471–476.

[36] G.D. Chryssikos, E.I. Kamitsos, A.P. Patsis, M.S. Bitsis, M.A. Karakassides, Devitrification of lithium metaborate: polymorphism and glass formation, J. Non-Cryst. Solids 126 (1990) 42–51.

[37] B.P. Dwivedi, M.H. Rahman, Y. Kumar, B.N. Khanna, Raman scattering study of lithium borate, J. Phys. Chem. Solids 54 (5) (1993) 162–625.

[38] G.D. Chryssikos, M.S. Bitsis, J.A. Kapoutsis, E.I. Kamitsos, Vibrational investigation of lithium metaborate–metaaluminate glasses and crystals, J. Non-Cryst. Solids 217 (1997) 278.

[39] M. Ganguli, K.J. Rao, Structural role of PbO in $Li_2O$–PbO–$B_2O_3$ glasses, J. Solid State Chem. 145 (1999) 65.

[40] M.D. Ingram, Ionic conductivity in glasses, Phys. Chem. Glasses 28 (1987) 215.

[41] S. Ramesh, A.K. Arof, Structural role of PbO in $Li_2O$–PbO–$B_2O_3$ glasses, Mater. Sci. Eng. B 85 (2001) 11–15.

[42] J. Maier, S. Prill, B. Reichert, Space charge effects in polycrystalline, micro polycrystalline and thin film samples: application to AgCl and AgBr, Solid State Ionics 28 (1988) 1465.

[43] A. Mogus-Milankovic, A. Santic, M. Karabulut, D.E. Day, Study of electrical properties of $MoO_3$–$Fe_2O_3$–$P_2O_5$ and SrO–$Fe_2O_3$–$P_2O_5$ glasses by impedance spectroscopy, J. Non-Cryst. Solids 330 (2003) 128.

[44] A.K. Jonscher, Dielectric Relaxation in Solids, Chelsea Dielectric Press, London, 1983.

[45] J.R. Macdonald (Ed.), Impedance Spectroscopy – Emphasising Solid Materials and Systems, John Wiley & Sons, New York, 1987.

[46] A.K. Jonscher, The 'universal' dielectric response, Nature 267 (1977) 673–679.

[47] M.I. Mohammed, K. Abd-allah, M.Y. Hassaan, The conduction mechanism and dielectric behavior of sodium borate glass containing Fe and Bi ions, Egypt. J. Solids 27 (2004) 299.
[48] K.H. Mahmoud, F.M. Abdei-Rahim, K. Atef, Y.B. Saddeek, Dielectric dispersion in lithium bismuth–borate glasses, Curr. Appl. Phys. 11 (2011) 55–60.
[49] A.K. Jonscher, Universal Relaxation Law, Chelsea Dielectric Press, London, 1996.
[50] P.B. Macedo, C.T. Moynihan, R. Bose, Role of ionic diffusion in polarization in vitreous ionic conductors, Phys. Chem. Glasses 13 (1972) 171–179.
[51] R. Balaji Rao, R.A. Gerhardt, Effect of alkaline earth modifier ion on the optical, magnetic and electrical properties of lithium nickel borate glasses, Mater. Chem. Phys. 112 (2008) 186–197.
[52] C.T. Moynihan, L.P. Boesch, N.L. Laberage, Decay function for the electric field relaxation in vitreous ionic conductors, Phys. Chem. Glasses 14 (1973) 122–126.